NRIAG JOURNAL OF ASTRONOMY AND GEOPHYSICS
2020, VOL. 10, NO. 1, 10–22
https://doi.org/10.1080/20909977.2020.1846246

OPEN ACCESS Check for updates

Development of natural polymer/metal oxide nanocomposite reinforced with graphene oxide for optoelectronic applications

Hend A. Ezzat[a], Maroof A. Hegazy[a], Nadra A. Nada[b], Osama Osman[c] and Medhat A. Ibrahim[c]

[a]Nano Technology Unit, Space Lab, Solar and Space Research Department, National Research Institute of Astronomy and Geophysics (Nano NRIAG), Helwan, Cairo, Egypt; [b]Physics Department, Faculty of Women for Arts, Science and Education, Ain Shams University, Cairo, Egypt; [c]Molecular Spectroscopy and Modeling Unit, Spectroscopy Department, National Research Centre, Dokki, Giza, Egypt

ABSTRACT

Nanocomposite natural polymer/metal oxide (NP/MO) is an attractive new technology for numerous applications as sensors, coatings, electronic devices, adhesives and optical circuits. NP includes cellulose Cel, chitosan Cs and sodium alginate NaAlg while MO are ZnO and CuO. Furthermore, modification of NP/MO with graphene oxide (GO) increases efficiency and stability of NP/MO in all its applications and fields. Theoretical calculations using density functional theory (DFT) were conducted to study the effect of using GO on electronic properties and thermal stability of NP/MO. Total dipole moment (TDM), HOMO/LUMO band gap energy (ΔE) and molecular electrostatic potential (MESP) were computed for the interaction of GO with NP/MO at B3LYP/LANL2DZ. Moreover, QSAR descriptors were also calculated for the same interactions. It was found that GO/NP/MO structure is auspicious for new materials with the efficient expense, more stable (physically and chemically), thermally stability and more sensitive, particularly GO/Cel/MO and GO/Cs/MO, while GO/Nav Alg/MO did not make significant changes.

ARTICLE HISTORY
Received 23 June 2020
Revised 16 August 2020
Accepted 26 October 2020

KEYWORDS
Graphene oxide; natural polymer/metal oxide; electronic properties; B3LYP/LANL2DZ AND QSAR

1. Introduction

Polysaccharides are natural compounds extracted from natural resources. For example, Cel, Cs and NaAlg have free amino and hydroxyl groups capable of chelating metal ions, and their lone pairs of electrons are easily used to coordinate bonding with surrounding structures (Crawford 1981). Cel is described chemically as β 1,4-linked d-glucose rings (Lefebvre and Gray 2005). It has many important properties as it is biocompatible, recyclable, biodegradable and renewable polysaccharides which make it significant in several applications (Updegraff 1969; Dufresne 2008, 2013). Also, Nano cellulose isolated from Cel reveals a remarkable increase in Cel properties (Ashrafi and Azadi 2015). Another polysaccharide polymer which has nearly similar characteristics of other polysaccharides is Cs. Cs chemical structure is a co-polymer of N-glucosa, hd. 'k, jl. mine and N-acetyl-glucosamine linked by β-(1′4)-glycosidic bonds which is a derivative of the N-acetylation of chitin in hot alkaline media (Saboktakin et al. 2011; Sahariah and Másson 2017). It has also been extensively changed chemically, such modifications allow it to fulfil different biological and medical needs according to the active functional groups distinctive to it (Rioux et al. 2007; Lin et al. 2016; El et al. 2018; Yu et al. 2019). Similarly, NaAlg is a carbohydrate biopolymer with the chemical formula (C6H7Na1/2O6)n, derived from brown algae, which serves in a broad variety of applications with special properties (Gomez et al. 2009; Kovalenko et al. 2011; Jmiai et al. 2018; Laffleur and Röttges 2019).

Organic/inorganic composite structures may also give an attractive performance by incorporating the advantages of organic and inorganic products into successful electronic devices (Kazi and Yamamoto 2019). Nanocomposites are promising in various applications and fields such as sensors, coatings, microelectronic processing, optical integrated circuits and adhesives (Wang et al. 2019). It became known that nanocomposites would find useful applications in areas such as actuators, sensors, fuel cell capacitors and self-regulating heaters (Arena et al. 2017). The synthesis of Cel/ZnO hybrid nanocomposite has also enhanced UV sensing properties, various applications as a photocatalyst, medicine and biology (Hashim et al. 2019; Ibrahim et al. 2019a; Mun et al. 2017; Vanitjinda et al. 2019). Moreover, an easy-to-construct technique that has demonstrated excellent sound-adsorption, mechanical and flame-retardant enhancement of Cel-based composite aerogels is through the introduction of aluminium hydroxide nanoparticles (AH NPs) into Cel gels by the sol-gel process. This Cel nanocomposite gives a future promising applications as green engineering materials (Khalid et al. 2017).

CONTACT Hend A. Ezzat hend_ahmed16@yahoo.com; hend.ezzat@nriag.sci.eg Nano Technology Unit, Space Lap, Solar and Space Department, National Research Institute of Astronomy and Geophysics, Helwan, Cairo 11421, Egypt

© 2020 The Author(s). Published by Informa UK Limited, trading as Taylor & Francis Group.
This is an Open Access article distributed under the terms of the Creative Commons Attribution License (http://creativecommons.org/licenses/by/4.0/), which permits unrestricted use, distribution, and reproduction in any medium, provided the original work is properly cited.

Furthermore, a novel X-ray shielding was achieved with BaSO4/Cel nanocomposite membrane (Lefatshe et al. 2017). Cs nano-metallic oxide composite is one of the least exploited materials for electrical application (He et al. 2018). Cs/ZnO nanocomposite enhances the dielectric properties, mechanical properties and thermal stability. Cs/ZnO nanocomposite film results showed that the values of both conductivity and dielectric constant were increased after the addition of nano ZnO (Jianga et al. 2019).

Electrical, optical and mechanical properties of Cs/GNP and Cs/MWCNT biocomposite films have been greatly enhanced, qualifying them to be applied for food processing, ultraviolet safety and biomedical applications that the biological activity increasing with increase nano filler (Marroquin et al. 2013). GO/Cs composite film could be an excellent proton-conducting electrolyte with a high specific capacity and used to manufacture multi-gate electrical double-layer transistors (Rahman et al. 2018). GO/Cs/NMO composite is an opportunity and challenge for realistic applications in the area of sensing, catalysis and energy storage (Feng et al. 2016; Mergen et al. 2020). In order to improve mechanical strength and ultraviolet shielding properties, GO was integrated as a functional nanofiller into a NaAlg matrix to form a composite film using a solvent-casting process (Majidi et al. 2020).

Theoretical calculations using molecular dynamics, termed molecular modeling, became nowadays an effective tool for studying nanomaterials (Jena et al. 2020; Hu et al., 2016; Bayoumy et al. 2018; Fahmy et al. 2020; Ibrahim et al. 2019b). Studying chemical, physical and electronic properties of several systems was carried out using different levels and theories of molecular modeling (Abdel-Bary et al. 2020; Badry et al. 2019; Bayoumy et al. 2019b; Ibrahim and Mahmoud 2009; Bayoumy et al. 2019a). Molecular modeling TDM, ΔE, and MESP parameters are important to study polymeric systems as synthetic and/or natural and their polymer nanocomposite matrices (Politzer et al. 1985; Ibrahim and Elhaes 2005; Sahin et al. 2015; Refaat et al. 2019; Ezzat et al. 2019; Abdelsalam et al. 2019).

Physical and electronic properties could be studied to investigate the reactivity of considered structure (Frisch et al. 2010; Becke 1993; Lee et al. 1988; Miehlich et al. 1989; Abdelsalam et al. 2018b). According to quantum mechanics, there is another theoretical calculation that is used to study the molecular activity which is correlated with molecular modeling, and is called QSAR. QSAR calculations are used to study biological activity and physicochemical properties of the chemical molecules, and is used in engineering, chemical and biological sciences (Abdelsalam et al. 2018a; Hansch and Leo 1995).

QSAR descriptors that are used for calculations give various properties such as structural, chemical and physical properties for studied molecules. In addition, there is a variety of common descriptors, such as those describing electronic effects within the molecules and the accordance of lipophilicity (Welsh et al. 2007; Elhaes et al. 2012).

The electronic properties of NP such as Cel, Cs and NaAlg is supposed to be enhanced is after composite formation with ZnO and/or CuO. Based on the above considerations, DFT calculations were carried out to study the impact of GO on the electronic properties and thermal stability of some polysaccharide/metal oxides NP/MO nanocomposite. For each structure the total dipole moment TDM, band gap energy ΔE and molecular electrostatic potential MESP were calculated at B3LYP/LANL2DZ. Thne some QSAR descriptors have also been determined for the same structures.

2. Computational details

Model structures were built for the natural polymer such as Cel, Cs and NaAlg as well as their adsorb state interaction with metal oxides (ZnO and CuO) through oxygen atom O. further models were built for studying the effect of GO on NP interacted with MO forming nanocomposite. DFT was applied for postulated structures calculated at B3LYP level with a LANL2DZ basis set. Electronic properties were studied for all structures by calculating TDM and ΔE at the same level of theory. Another important parameter for the postulated structures electronic properties study is MESP. MESP was also computed for all structures using the same level of theory. QSAR thermodynamic properties were also computed for the postulated structures at PM6 level. All calculations were computed using the software at Spectroscopy Department, Physics Division, National Research Centre, NRC.

3. Results and discussion

3.1. Model structure and electronic properties

NP represented by Cel, Cs and NaAlg to investigate the transformation occur in electronic properties of NP in the presence of MO, then studying the effect of GO on NP/MO electronic properties. The postulated structures were divided into three groups. The first group is supposed to represent adsorption Cel interaction with MO such as ZnO and CuO through O atom and GO adsorption with Cel/MO composite. The second group represents adsorption Cs interaction with MO such as ZnO and CuO through O atom and GO adsorption with Cs/MO composite. The third group represents adsorption NaAlg interaction with MO such as ZnO and CuO through

O atom and GO adsorption with NaAlg/MO composite. DFT was used for the postulated structures and calculated at B3LYP level with a LANL2DZ basis set. By measuring TDM and ΔE at the same level of theory, electronic properties were studied for all structures. Figure 1 represents optimised structure for base materials and ΔE as Cel, Cs, NaAlg and GO.

For Cel, Cs, NaAlg and GO-based materials, the distribution of molecular orbitals tends to be homogeneous around the molecule. Table 1 describes TDM and ΔE energy for Cel, Cs, NaAlg and GO-based materials. For Cel, TDM were recorded at 2.644 Debye and 13.621 eV for ΔE. Furthermore, 4.094 Debye and 2.571 eV were registered for Cs TDM for ΔE respectively. In addition, 16.846 Debye and 0.366 eV respectively were registered for TDM and ΔE respectively in the case of NaAlg. Finally, 2.711 Debye and 0.450 eV were registered for TDM and ΔE of GO.

3.2. Cel/MO and GO/Cel/MO

The first group is expected to reflect adsorption Cel interaction with ZnO and CuO via the O atom and GO adsorption with Cel/MO composite. Optimised structure and ΔE for the supposed structures were illustrated in Figure 2.

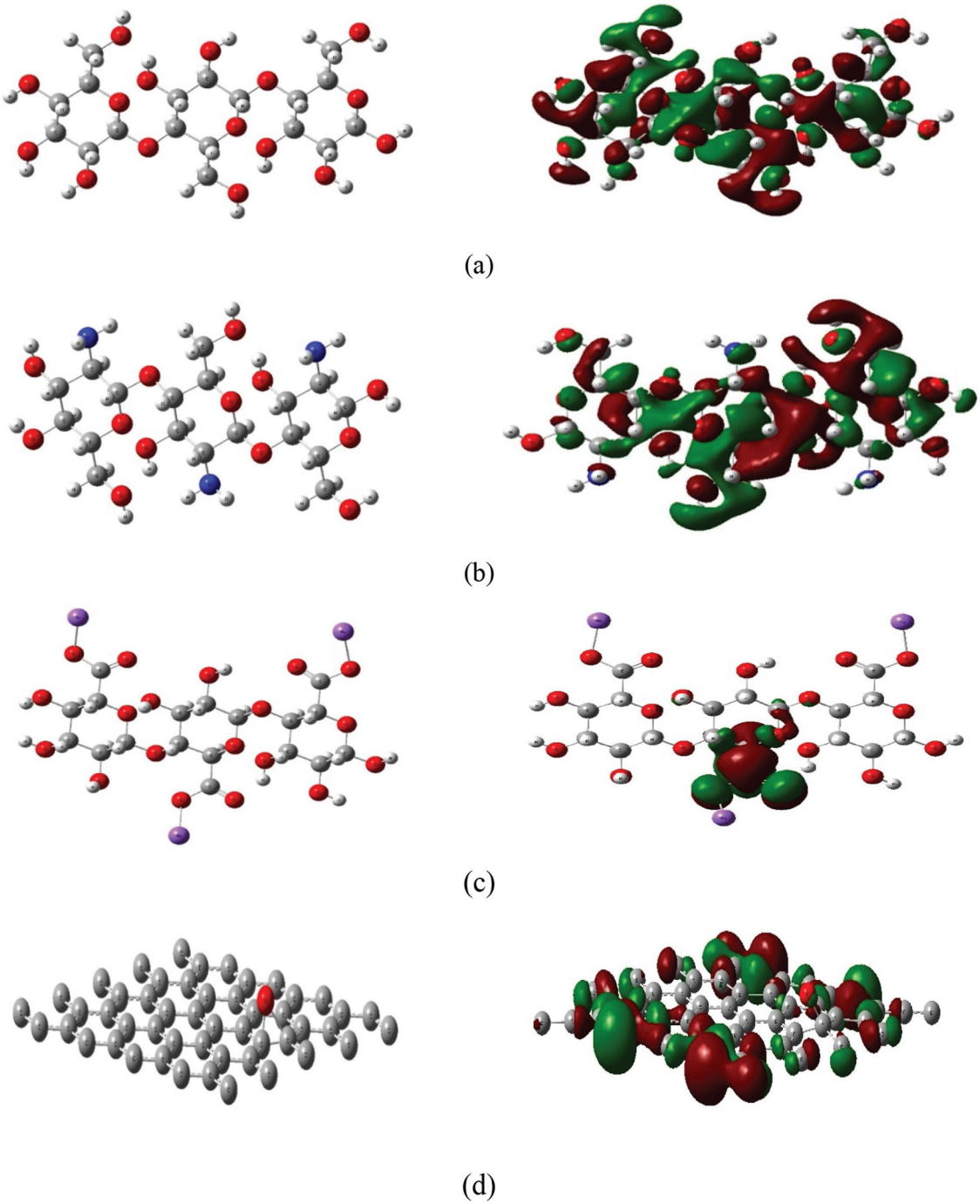

Figure 1. Base materials optimised structure and ΔE for (a) Cellulose, (b) Chitosan, (c) Sodium alginate and (d) Graphene oxide.

Table 1. Optimised TDM (Debye) and ΔE (eV) using B3LYP/LANL2DZ for Cel, Cs, NaAlg and GO.

Structure	TDM	ΔE
Cel	2.644	13.621
Cs	4.094	2.571
NaAlg	16.846	0.366
GO	2.711	0.450

Table 2 demonstrates the TDM and ΔE variation for Cel group. For Cel/MO, TDM increased from 2.644 Debye for Cel only to 15.787 and 24.005 Debye for Cel/OZn and Cel/OCu, while ΔE decreased from 13.621 eV to 0.278 and 0.287 eV, respectively. It was noticed in the case of studying the impact of GO on the Cel that TDM was increased to 28.524 Debye and ΔE decreased to 0.360 eV, but for GO/Cel/MO, TDM changed to 36.766 and 20.895 Debye, and ΔE also changed to 0.350 and 0.246 eV for GO/Cel/OZn and GO/Cel/OCu, respectively. From all data of Cel group, GO/Cel/OCu recorded a significant enhancement in its electrical properties.

3.3. Cs/MO and GO/Cs/MO

Similarly, the Cs group is supposed to represent electrostatic Cs interaction with ZnO and CuO via the O atom and GO electrostatic interaction with Cs/MO composite. Table 3 shows the TDM and ΔE variation for Cs group. Optimised configurations and energy difference of ΔE for the proposed structures are shown in Figure 3. TDM of Cs/MO increased to 15.392 and 18.524 Debye, while ΔE decreased to 0.357 and 0.385 eV for Cs/OZn and Cs/OCu, respectively. While investigating the effect of GO on Cs, it was observed that the TDM was

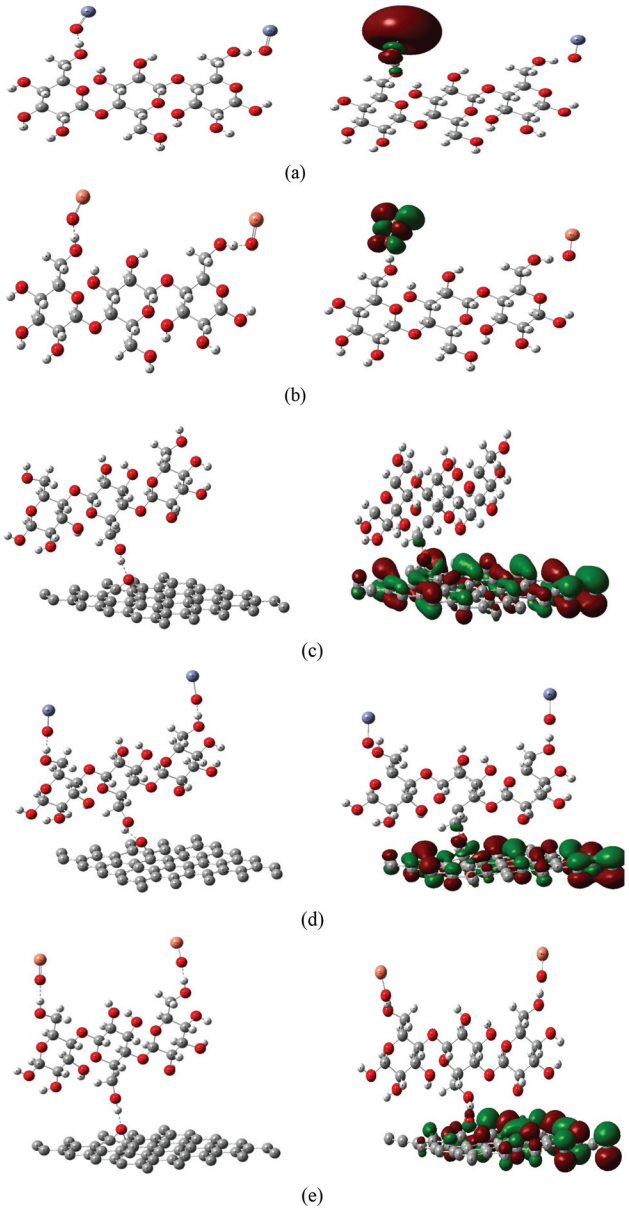

Figure 2. Cel/MO and GO/Cel/MO models optimised ΔE as (a) Cel/ZnO, (b) Cel/CuO, (c) GO/Cel, (d) GO/Cel/ZnO and (e) GO/Cel/CuO.

Table 2. Optimised TDM (Debye) and ΔE (eV) using B3LYP/LANL2DZ for Cel/ZnO, Cel/CuO, GO/Cel, GO/Cel/ZnO and GO/Cel/CuO.

Structure	TDM	ΔE
Cel/OZn	15.787	0.278
Cel/OCu	24.005	0.287
GO/Cel	28.524	0.360
GO/Cel/OZn	36.766	0.350
GO/Cel/OCu	20.895	0.246

Table 3. Optimised TDM (Debye) and ΔE (eV) using B3LYP/LANL2DZ for Cs/ZnO, Cs/CuO, GO/Cs, GO/Cs/ZnO and GO/Cs/CuO.

Structure	TDM	ΔE
Cs/OZn	15.392	0.357
Cs/OCu	18.524	0.385
GO/Cs	36.824	0.347
GO/Cs/OZn	34.850	0.266
GO/Cs/OCu	17.424	0.294

increased to 36.824 Debye and ΔE decreased to 0.347 eV. GO/Cs/MO TDM improved to 34.850 and 17.424 Debye and ΔE also adjusted to 0.266 and 0.294 eV corresponding to GO/Cs/OZn and GO/Cs/OCu, respectively. A major improvement in electrical properties was reported for GO/Cs/OZn of Cs group.

3.4. NaAlg/MO and GO/NaAlg/MO

Finally, the NaAlg group is supposed to reflect the electrostatic interaction of NaAlg with ZnO and CuO, and the electrostatic interaction of GO with O atom with NaAlg/MO composite. Figure 4 shows the optimised structure and energy differential of ΔE for the expected structure. TDM and ΔE calculated for the NaAlg group are listed in Table 4. NaAlg/MO changed TDM and ΔE to 26.778 Debye and 28.533 Debye, and 0.389 eV and 0.346 eV for NaAlg/OZn and NaAlg/OCu, respectively. Upon GO interaction with NaAlg, the TDM was changed to 47.967 Debye and ΔE also changed to 0.390 eV. GO/NaAlg/MO TDM upgraded to 43.208 and 47.238 Debye, while ΔE did not make a significant change as 0.385 and 0.309 eV for GO/NaAlg/OZn

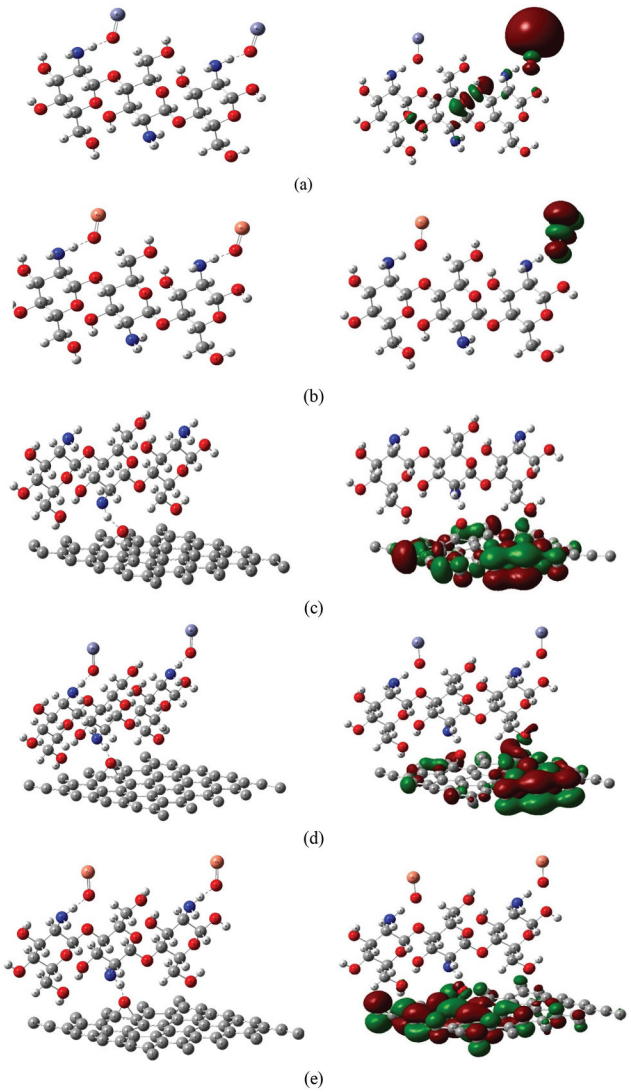

Figure 3. Cs/MO and GO/Cs/MO models optimised ΔE as (a) Cs/ZnO, (b) Cs/CuO, (c) GO/Cs, (d) GO/Cs/ZnO and (e) GO/Cs/CuO.

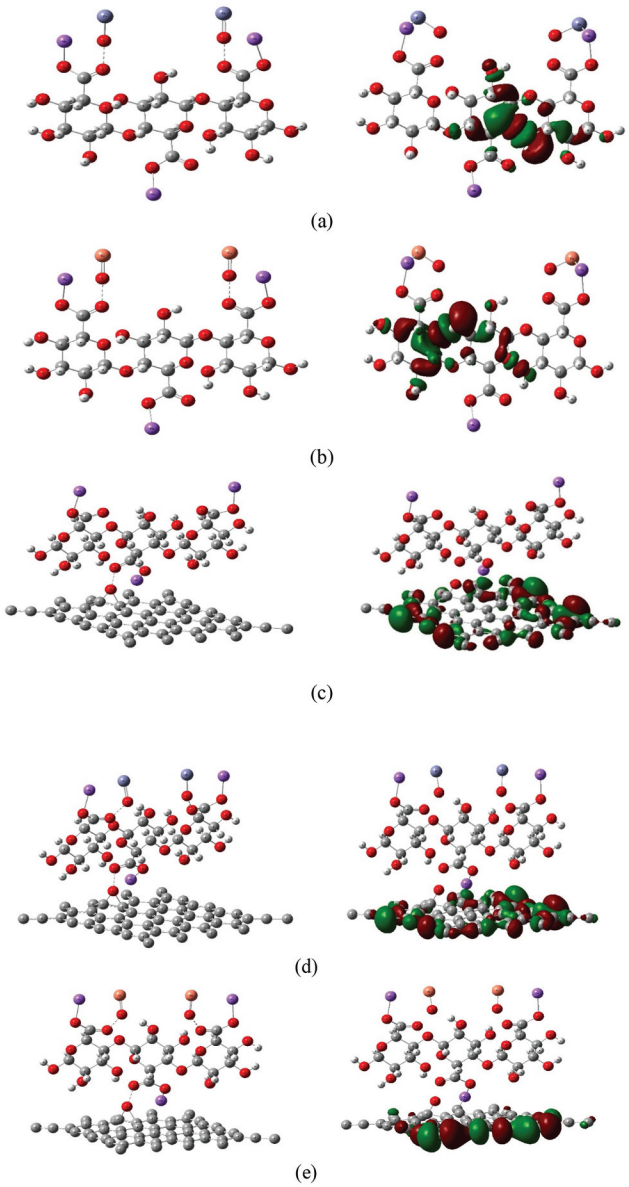

Figure 4. NaAlg/MO and GO/NaAlg/MO models optimised ΔE as (a) NaAlg/ZnO, (b) NaAlg/CuO, (c) GO/NaAlg, (d) GO/NaAlg/ZnO and (e) GO/NaAlg/CuO.

and GO/NaAlg/OCu, respectively. Accordingly, GO could not make an important change in NaAlg electrical properties.

3.5. Molecular Electrostatic Potential (MESP)

The MESP is another significant parameter used for the study of the postulated structures describing the electronic charge transfer, which defines the measurement of the adjacent nucleus, charge and electron concentration at a given position. MESP is often computed for all systems that use the same theory. MESP is commonly used as a reactivity indication of the most possible area for nucleophilic and electrophilic interaction. Figures 5–8 represent the contour and 3D total density of MESP. In the MESP map, the red colour corresponds to the electron-rich (negative) region, the blue colour corresponds to the electron-poor (positive) region, and the green colour shows zero electrostatic potential. Negative locations inside a specific molecule are marked by a red colour that is related to the electrophilic reactivity of the molecule. Nevertheless, the positive blue regions as shown in the figure are linked to the nucleophilic reactivity of the molecule. The electron concentrations on the MEP surface are shown in various colours.

Table 4. Optimised TDM (Debye) and ΔE (eV) using B3LYP/LANL2DZ for NaAlg/OZn, NaAlg/OCu, GO/NaAlg, GO/NaAlg/OZn and GO/NaAlg/OCu.

Structure	TDM	ΔE
NaAlg/OZn	26.778	0.389
NaAlg/OCu	28.533	0.346
GO/NaAlg	47.967	0.390
GO/NaAlg/OZn	43.208	0.385
GO/NaAlg/OCu	47.238	0.309

Table 5. Calculated propertes using semiempirical theory at PM6 level as charge, total energy (ev), heat of formation (K cal/mol), ionisation potential (eV), Log P, polarisability, molar refractive (MR), molecular weight (MW), surface area and volume. For the three groups of the natural polymer with metal oxides and GO: Cel, Cel/OZn,Cel/OCu, GO/Cel/OZnO, GO/Cel/OCu, Cs, Cs/OZn, Cs/OCu, GO/Cs/OZn, GO/Cs/OCu, NaAlg, NaAlg/OZn, NaAlg/OCu, GO/Na Alg/OZn and GO/Na Alg/OCu.

Structure	Charge	T E (ev)	HF	IP(eV)	Log P	Polarisability	MR	MW	Surface Area	Volume
Cel	0	−8705.915	−714.150	−10.449	−4.194	30.123	100.750	504.437	428.61	371.58
Cel/OZn	0	−9458.157	−764.266	−10.373	−4.897	34.965	103.636	667.254	468.86	420.26
Cel/OCu	0	−11726.312	−686.911	−8.444	−4.897	34.781	103.636	663.528	465.3	414.1
GO/Cel	0	−2996.885	712.101	−8.404	−4.533	138.929	258.491	1120.971	849.6	791.87
GO/Cel/OZn	0	−16526.348	688.868	−8.959	−5.236	160.057	261.377	1283.788	955.18	864.44
GO/Cel/OCu	0	−10532.952	−364.334	−7.295	−5.236	132.195	261.377	1280.062	909.78	844.38
Cs	0	−8479.409	−578.295	−9.720	−5.236	30.718	105.723	501.483	444.26	387.58
Cs/OZn	0	−9201.264	−612.992	−8.929	−5.939	47.961	108.608	664.300	529.67	468.05
Cs/OCu	0	−11171.690	−510.222	−9.182	−5.939	34.607	108.608	660.574	526.73	443.7
GO/Cs	0	−2698.839	896.141	−8.880	−5.575	135.453	263.464	1118.017	873.57	813.21
GO/Cs/OZn	0	−7191.434	639.407	−8.243	−6.278	170.514	266.349	1280.834	933.87	868.75
GO/Cs/OCu	0	−8712.148	993.489	−8.084	−6.278	147.278	266.349	1277.108	967.08	873.16
Na Alg	0	−9535.094	−969.755	−9.149	−3.532	33.420	97.569	612.333	424.85	365.2
Na Alg/OZn	0	−10264379	−1186.330	−8.685	−4.235	43.437	100.455	775.150	514.82	449.05
Na Alg/OCu	0	−12586.648	−1651.326	−8.688	−4.235	41.339	100.455	771.424	479.59	418.87
GO/Na Alg	0	−17272.612	186.360	−8.541	−3.871	140.143	255.311	1228.868	838.49	782.17
GO/NaAlg/OZn	0	−8391.903	−24.109	−7.708	−4.574	148.708	258.196	1391.684	918.86	866.06
GO/Na Alg/OCu	0	−6447.348	−349.044	−7.926	−4.574	158.479	258.196	1387.958	879.64	825.57
GO	0	−7685.057	1508.272	−8.952	−0.339	105.182	157.741	616.534	459.08	444.18

Electron density values are raised in the following order: Red > Orange > Yellow > Green > Blue.

The MESP isosurface of GO/Cel/MO and GO/Cs/MO documented that the charges are equally dispersed in the whole molecules. However, it is obvious from the MESP statistics that there are no negative MESP regions located outside the GO/Cel/MO and GO/Cs/MO, and that only positive MESP regions are located inside them. In addition, it is evident that the highest positive region is mostly situated above the MO atoms (OZn and OCu), which are deemed ideal for nucleophilic attacks. The nucleophilic attacks are found to be more prevalent than electrophilic attacks owing to GO/Cel/MO and GO/Cs/MO. The results

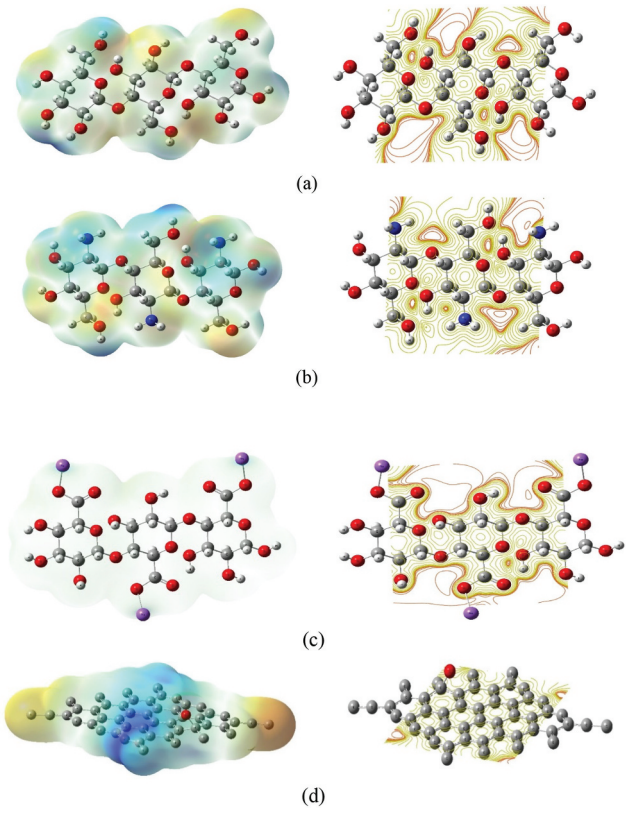

Figure 5. MESP of Base materials as total surface and contour respectively for (a) Cellulose, (b) Chitosan, (c) Sodium alginate and (d) Graphene oxide.

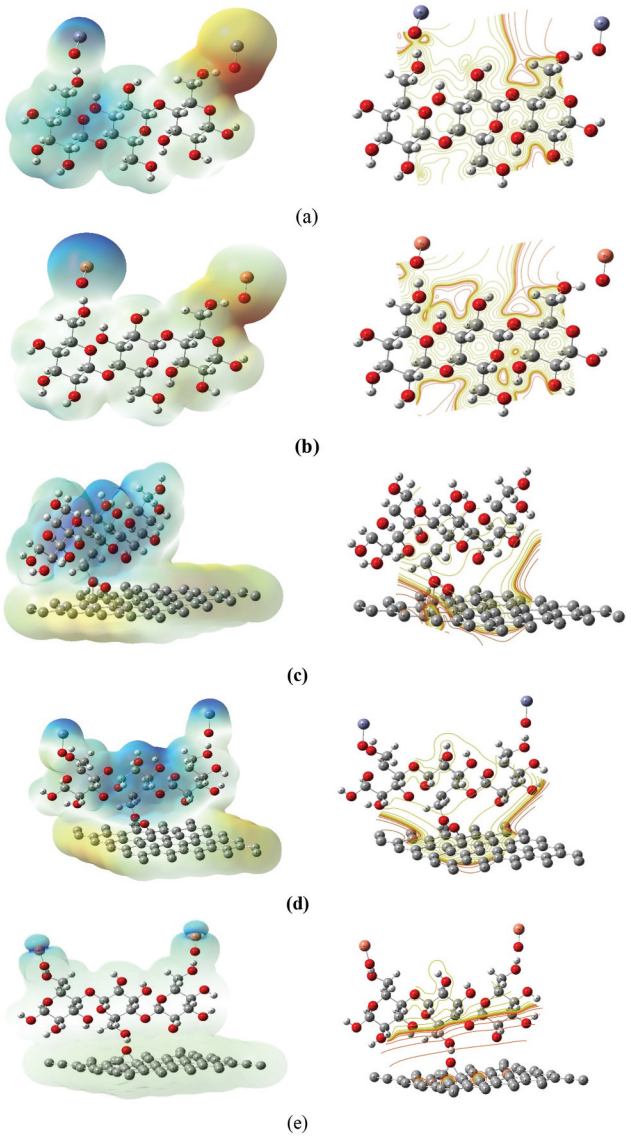

Figure 6. MESP of base materials as total surface and contour respectively for (a) Cel/ZnO, (b) Cel/CuO, (c) GO/Cel, (d) GO/Cel/ZnO and (e) GO/Cel/CuO.

obtained from MESP indicated that these structures were highly stable. For GO/NaAlg/MO, the MESP isosurface was neutral which is observed with yellow colour.

3.6. QSAR Calculations

Physical, electronic and QSAR properties were calculated for all proposed molecules. The resulting properties are shown in Table 1. QSAR properties are charge, total energy (TE), the heat of formation (HF), ionisation potential (IP), Log P, polarisability, molar refractive (MR), molecular weight (MW), surface area and volume.

Charge descriptor was equivalent to zero for all constructs that are an indicator of being in the ground state. Then, TE are calculated which TE characterise the structure stability. As TE value reduces the structure becomes known as a more stable structure. As shown in Table 5, TE for Cel in Cel group is equal to −8705.915 eV. Additionally, TE has improved with nanometal oxide as it declined for Cel/OZn and Cel/OCu to −9458.157 and −11726.312 eV, respectively. As well, GO decreased TE for Cel group to −16526.348 and −10532.952 eV for GO/Cel/OZn and GO/Cel/OCu, respectively, indicating that GO/Cel/MO is more stable structure especially Cel/OZn. Similarly, TE makes a small change for GO/Cs/MO from −8479.409 to −7191.434 and −8712.148 eV for GO/Cs/OZn and GO/Cs/OCu, respectively. Finally, TE for NaAlg group increased in the case of GO/NaAlg/MO from −9535.094 to −8391.903 and −6447.348 for GO/NaAlg/OZn and GO/NaAlg/OCu, respectively, which means that NaAlg/MO is more stable than GO/NaAlg/MO.

HF is a critical thermal descriptor that describes the energy generated as heat as atoms reside at

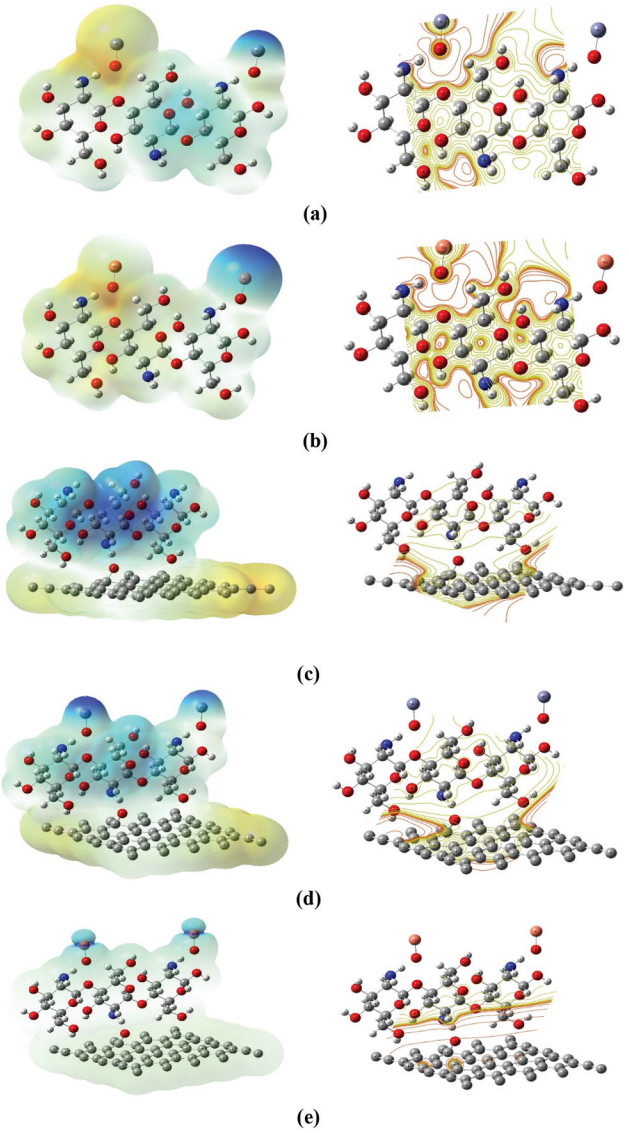

Figure 7. MESP of base materials as total surface and contour respectively for (a) Cs/ZnO, (b) Cs/CuO, (c) GO/Cs, (d) GO/Cs/ZnO and (e) GO/Cs/CuO.

theoretically infinite distances connect and produce a certain molecule. As far as HF is concerned, it can be defined as the shifting occurring in the enthalpy after the creation of a single mole of a substance from its components in its natural and stable state under atmospheric standard conditions at a given temperature. For the heat of the material, for a particular substance, the amount of heat produced or absorbed into a single mole is defined. Referring to Table 5 data, the lowest HF values in the three groups were GO/Cel/OCu, GO/Cs/OZn and GO/Na Alg/OCu which recorded a minimal amount of energy to be produced.

Another essential QSAR descriptor is the IP that characterises the reactivity of the compound. IP is defined as the energy required for the compound to be ionised. When the IP benefit reduces, the reactivity of chemical substance increases. The data relationship between GO and NP/MO will not allow a major difference in the IP.

The descriptor that represents the hydrophilicity of the chemical substance is the logarithm of the partition coefficient (log P). Log P is equal to the amount of dissolving content in organic solution to dissolving in aqueous solvents. Subsequently, positive Log P values are related to hydrophobic compounds and negative values indicate hydrophilic compounds. For our group products, all the suggested compositions had a negative log P, meaning that the substances are hydrophilic (water soluble). GO/NP/MO proposed structures are slightly more hydrophilic than NP.

Polarisability can be characterised as the ease with which the chemical structure tends to be polarised in response to external forces. It somehow reflects the reactivity of the chemical structures, and it depends on their volume. Polarisability for our model structures make a significant increase for GO/Cel/OZn, GO/Cs/OZn, GO/Na Alg/OZn, GO/Na Alg/OCu which means that these models are more reactive than others.

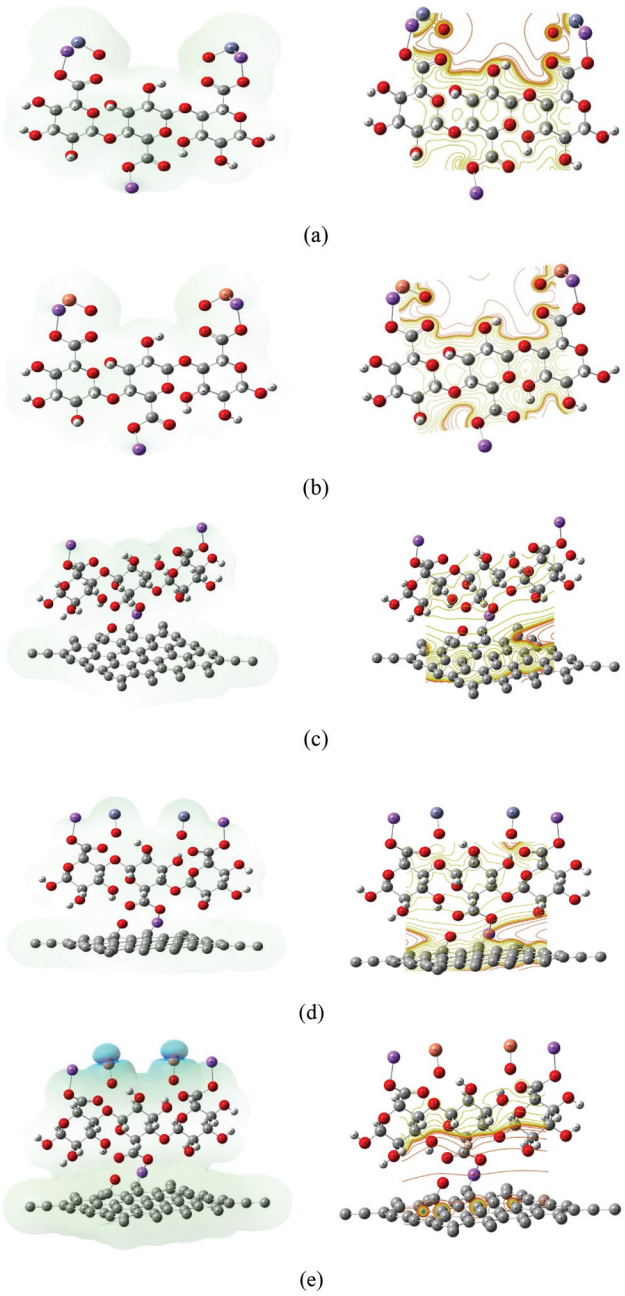

Figure 8. MESP of base materials as total surface and contour respectively for (a) NaAlg/ZnO, (b) NaAlg/CuO, (c) GO/NaAlg, (d) GO/NaAlg/ZnO and (e) GO/NaAlg/CuO.

Likewise, surface region and volume are the physical parameters of the QSAR. In addition, the MR is a descriptor that measures the overall polarisation of the mole of the material. The greater the MR, the greater the reactivity of the structure. As described in Table 5, GO/NP/MO recorded more reactive structures than NP only.

All QSAR, geometrical and thermal properties indicated that GO increases the physical, thermal stability and reactivity of NP/MO. These findings make the proposed GO / NP / MO structure a promising new material that is cost-effective, more stable (physically and chemically), thermally stable and more reactive especially GO/Cel/MO and GO/Cs/MO while GO/NaAlg/MO did not make a significant change.

4. Conclusions

Theoretical investigations were carried out to evaluate the effect of GO on the electronic properties and thermal stability of certain NP/MO nanocomposite polysaccharides using DFT. All the proposed structure of GO with NP/MO were conducted to calculate TDM, ΔE and MESP were measured at B3LYP level with a LANL2DZ basis set. QSAR descriptors were also calculated for the same interactions in order to

study the physical, chemical and thermal stability. Electronic properties recorded a major enhancement for GO/Cel/OCu and GO/Cs/OZn. Correspondingly, QSAR, geometric and thermal properties calculations ensured that GO increased NP/MO physical, thermal stability and reactivity which leads to that the new materials with GO/NP/MO structure have significant properties as an efficient expense, more stable (physically and chemically), thermally stable and more sensitive, particularly GO/Cel/MO and GO/Cs/MO, while GO/NaAlg/MO did not make significant changes. For cheap materials such as polysaccharides, metal oxide could enhance its electronic properties. While graphene which is a promising electronic material consisting of sp2 carbon atom monolayers with a 2D honeycomb lattice gives the polysaccharides/metal oxides further enhancements. Collecting the TDM, ΔE, MESP and QSAR descriptors, one can conclude that the studied combination of NP/MO/GO provides excellent optoelectronic applications as a result of the combination of high carrier mobility, active sites and reactivity. Nanocomposite of NP/MO/GO is an attractive new technology for numerous applications as sensors, coatings, electronic devices, adhesives and optical circuits. Following the proper experimental procedure for preparation of the proposed combination, one can dedicate this structure for optoelectronic application in many areas.

Disclosure statement

No potential conflict of interest was reported by the authors.

ORCID

Hend A. Ezzat http://orcid.org/0000-0002-2370-3038
Osama Osman http://orcid.org/0000-0002-9977-3964
Medhat A. Ibrahim http://orcid.org/0000-0002-9698-0837

References

Abdel-Bary AS, Tolan DA, Nassar MY, Taketsugu T, El-Nahas AM. 2020. Chitosan, magnetite, silicon dioxide, and graphene oxide nanocomposites: synthesis, characterization, efficiency as cisplatin drug delivery, and DFT calculations. Int J Biol Macromol. 154:621–633. doi:10.1016/j.ijbiomac.2020.03.106.

Abdelsalam H, Elhaes H, Ibrahim MA. 2018a. Tuning electronic properties in graphene quantum dots by chemical functionalization: density functional theory calculations. Chem Phys Lett. 695:138–148. doi:10.1016/j.cplett.2018.02.015.

Abdelsalam H, Elhaes H, Ibrahim MA. 2018b. First principles study of edge carboxylated graphene quantum dots. Physica B. 537:77–86. doi:10.1016/j.physb.2018.02.001.

Abdelsalam H, Saroka VA, Ali M, Teleb NH, Elhaes H, Ibrahim MA. 2019. Stability and electronic properties of edge functionalized silicene quantum dots: A first principles study. Physica E Low Dimens Syst Nanostruct. 108:339–346. doi:10.1016/j.physe.2018.07.022.

Arena A, Scandurra G, Ciofi C. 2017. Copper oxide chitosan nanocomposite: characterization and application in non-enzymatic hydrogen peroxide sensing. Sensors-Basel. 17(10):2198.

Ashrafi H, Azadi A. 2015. Chitosan-based hydrogel nanoparticle amazing behaviors during transmission electron microscopy. Int J Biol Macromol. 84:31–34. doi:10.1016/j.ijbiomac.2015.11.089.

Badry R, El-Khodary S, Elhaes H, Nada N, Ibrahim M. 2019. On the molecular modeling analyses of sodium carboxymethyl cellulose treated with acetic acid. Lett ApplNanoBioScience. 8(2):553–557.

Bayoumy AM, El-Sayed EM, Omar A, Ibrahim M. 2018. Emerging applications of chitosan: from biology to environment. Biointerface Res Appl Chem. 8(4):3368–3380.

Bayoumy AM, Refaat A, Yahia IS, Zahran HY, Elhaes H, Ibrahim MA, Shkir M. 2019a. Functionalization of graphene quantum dots (GQDs) with chitosan biopolymer for biophysical applications. Opt Quantum Electron. 52:1–14.

Bayoumy AM, Youssif G, Elgohary EA, Husien S, Salah El Deen H, Albeltagy NM, Abdelnaby DM, Medhat A, Elhaes H, Ibrahim MA. 2019b. Impact of solvation on the geometrical parameters of some amino acids. Lett ApplNanoBioScience. 8(2):567–570.

Becke AD. 1993. Density-functional thermochemistry. III. The role of exact exchange. J Chem Phys. 98:5648–5652. doi:10.1063/1.464913.

Crawford RL. 1981. Lignin biodegradation and transformation. New York (NY): John Wiley and Sons; p. 154.

Dufresne A. 2008. Polysaccharide nano crystal reinforced nanocomposites. Can J Chem. 86(6):484–494. doi:10.1139/v07-152.

Dufresne A. 2013. Nanocellulose: a new ageless bionanomaterial. Mater Today. 16(6):220–227. doi:10.1016/j.mattod.2013.06.004.

El KH, Belaabed R, Addaou A, Laajeb A, Lahsini A. 2018. Extraction chemical modification and characterization of chitin and chitosan. Int J Biol Macromol. 120:1181–1189. doi:10.1016/j.ijbiomac.2018.08.139.

Elhaes H, Osman O, Ibrahim M. 2012. Interaction of nano structure material with heme molecule: modelling approach. J Comput Theor Nanosci. 9(7):901–905. doi:10.1166/jctn.2012.2114.

Ezzat HA, Hegazy MA, Nada NA, Ibrahim MA. 2019. Effect of nano metal oxides on the electronic properties of cellulose, chitosan and sodium alginate. Biointerface Res Appl Chem. 9(4):4143–4149.

Fahmy A, Khafagy RM, Elhaes H, Ibrahim MA. 2020. Molecular properties of polyvinyl alcohol/sodium alginate composite. Bio Res Appl Chem. 10(1):4734–4739.

Feng P, Du P, Wan C, Shi Y 1, Wan Q. 2016. Proton conducting graphene oxide/chitosan composite electrolytes as gate dielectrics for new-concept devices. Sci Rep. 6:34065. doi:10.1038/srep34065.

Frisch MJ, Trucks GW, Schlegel HB, Scuseria GE, Robb MA, Cheeseman JR, Scalmani G, Barone V, Mennucci B, Petersson GA. 2010. Gaussian09, revisions D. 01 and B. 01. Wallingford (CT): Gaussian, Inc.

Gomez CG, Pérez Lambrecht MV, Lozano JE, Rinaudo M, Villar MA. 2009. Influence of the extraction–purification conditions on final properties of alginates obtained from brown algae (Macrocystis pyrifera). Int J Biol Macromol. 44(4):365–371. doi:10.1016/j.ijbiomac.2009.02.005.

Hansch C, Leo L. 1995. Exploring QSAR: fundamentals and applications in chemistry and biology. Washington: American Chemical Society.

Hashim A, Al-Attiyah Kh HH, Obaid SF. 2019. Modern developments of polymer blend/oxide nanocomposites for biomedical applications as antibacterial and radiation shielding materials: a review. Res J Agric & Biol Sci. 14(1):8–18.

He C, Huang J, Li S, Meng K, Zhang L, Chen Z, Lai Y. 2018. Mechanically resistant and sustainable cellulose-based composite aerogels with excellent flame retardant, sound-absorption, and superantiwetting ability for advanced engineering materials. ACS Sustainable Chem Eng. 6(1):927–936. doi:10.1021/acssuschemeng.7b03281.

Hu X, Zhang X, Tian M, Qu L, Zhu S, Han G. 2016. Robust ultraviolet shielding and enhanced mechanical properties of graphene oxide/sodium alginate composite films. J Compos Mater. 50(17):2365–2374. doi:10.1177/0021998315603227.

Ibrahim A, Elhaes H, Meng F, Ibrahim M. 2019a. Effect of hydration on the physical properties of glucose. Bio Res Appl Chem. 9(4):4114–4118.

Ibrahim ID, Jamiru T, Sadiku ER, Hamam Y, Alayli Y, Eze AA. 2019b. Application of nanoparticles and composite materials for energy generation and storage. ET Nanodielectrics. 2(4):115–122. doi:10.1049/iet-nde.2019.0014.

Ibrahim M, Elhaes H. 2005. Computational spectroscopic study of copper, cadmium, lead and zinc interactions in the environment. Int J Environ Pollut. 23(4):417–424. doi:10.1504/IJEP.2005.007604.

Ibrahim M, Mahmoud AA. 2009. Computational notes on the reactivity of some functional groups. J Comput Theor Nanos. 6(4):1523–1526. doi:10.1166/jctn.2009.1205.

Jena G, Anandkumar B, Vanithakumari SC, George RP, Philip J, Amarendra G. 2020. Graphene oxide-chitosan-silver composite coating on Cu-Ni alloy with enhanced anticorrosive and antibacterial properties suitable for marine applications. Prog Org Coat. 139:105444. doi:10.1016/j.porgcoat.2019.105444.

Jianga X, Zhua X, Chang C, Liuc S, Luoad X. 2019. X-ray shielding structural and properties design for the porous transparent BaSO4/cellulose nanocomposite membranes. Int J Biol Macromol. 139:793–800. doi:10.1016/j.ijbiomac.2019.07.186.

Jmiai A, El Ibrahimi B, Tara A, El Issami S, Jbara O, Bazzi L. 2018. Alginate biopolymer as green corrosion inhibitor for copper in 1 M hydrochloric acid: experimental and theoretical approaches. J Mol Struct. 1157:408–417. doi:10.1016/j.molstruc.2017.12.060.

Kazi GAS, Yamamoto O. 2019. Effectiveness of the sodium alginate as surgical sealant materials. Wound Med. 24(1):18–23. doi:10.1016/j.wndm.2019.02.001.

Khalid A, Khan R, Ul-Islam M, Khn T, Wahid F. 2017. Bacterial cellulose-zinc oxide nanocomposites as a novel dressing system for burn wounds. Carbohydr Polym. 164:214–221. doi:10.1016/j.carbpol.2017.01.061.

Kovalenko I, Zdyrko B, Magasinski A, Hertzberg B, Milicev Z. 2011. A major constituent of brown algae for use in high-capacity Li-Ion batteries. Sci. 334(6052):75–79. doi:10.1126/science.1209150.

Laffleur F, Röttges S. 2019. Mucoadhesive approach for buccal application: preactivated chitosan. Eur Polym J. 113:60–66. doi:10.1016/j.eurpolymj.2019.01.049.

Lee C, Yang W, Parr RG. 1988. Development of the Colle-Salvetti correlation-energy formula into a functional of the electron density. Phys Rev B. 37:785–789. doi:10.1103/PhysRevB.37.785.

Lefatshe K, Muiva CM, Kebaabetswe LP. 2017. Extraction of nanocellulose and in-situ casting of ZnO/cellulose nanocomposite with enhanced photocatalytic and antibacterial activity. Carbohydr Polym. 164:301–308. doi:10.1016/j.carbpol.2017.02.020.

Lefebvre J, Gray DG. 2005. AFM of adsorbed polyelectrolytes on cellulose I surfaces spin-coated on silicon wafers. Cellulose. 12:127–134. doi:10.1007/s10570-004-1574-0.

Lin T, Liu E, He H, Shin MC, Moon C, Yang VC, Huang Y. 2016. Nose-to-brain delivery of macromolecules mediated by cell-penetrating peptides. Acta Pharm Sin B. 6(4):352–358. doi:10.1016/j.apsb.2016.04.001.

Majidi HJ, Mirzaee A, Jafari SM, Amiri M, Shahrousvand M, Babaei A. 2020. Fabrication and characterization of graphene oxide-chitosan-zinc oxide ternary nano-hybrids for the corrosion inhibition of mild steel. Int J Biol Macromol. 148:1190–1200. doi:10.1016/j.ijbiomac.2019.11.060.

Marroquin JB, Rhee KY, Park SJ. 2013. Chitosan nanocomposite films: enhanced electrical conductivity, thermal stability, and mechanical properties. Carbohydr Polym. 92(2):1783–1791. doi:10.1016/j.carbpol.2012.11.042.

Mergen ÖB, Arda E, Evingür GA. 2020. Electrical, optical and mechanical properties of chitosan biocomposites. J Compos Mater. 54(11):1497–1510. doi:10.1177/0021998319883916.

Miehlich B, Savin A, Stoll H, Preuss H. 1989. Results obtained with the correlation energy density functionals of becke and Lee, Yang and Parr. Chem Phys Lett. 157:200–206. doi:10.1016/0009-2614(89)87234-3.

Mun S, Kim HC, Ko H-U, Zhai L, Kim JW, Kim J. 2017. Flexible cellulose and ZnO hybrid nanocomposite and its UV sensing characteristics. Sci Technol Adv Mater. 18(1):437–446. doi:10.1080/14686996.2017.1336642.

Politzer P, Laurence PR, Jayasuriya K. 1985. Molecular electrostatic potentials: an effective tool for the elucidation of biochemical phenomena. Environ Health Perspect. 61:191–202. doi:10.1289/ehp.8561191.

Rahman PM, Mujeeb VA, Muraleedharan K, Thomas SK. 2018. Chitosan/nano ZnO composite films: enhanced mechanical, antimicrobial and dielectric properties. Arabian J Chem. 11(1):120–127. doi:10.1016/j.arabjc.2016.09.008.

Refaat A, Ibrahim MA, Elhaes H, Badry R, Ezzat H, Yahia IS, Zahran HY, Shkir M. 2019. Geometrical, vibrational and physical properties of polyvinyl chloride nanocomposites: molecular modeling approach. J Theor Comput Chem. 18(8). doi:10.1142/S0219633619500378.

Rioux LE, Turgeon SL, Beaulieu M. 2007. Characterization of polysaccharides extracted from brown seaweeds. Carbohydr Polym. 69(3):530–537.

Saboktakin MR, Tabatabaie RM, Maharramov A, Ramazanov MA. 2011. Synthesis and characterization of pH-dependent glycol chitosan and dextran sulfate nanoparticles for effective brain cancer treatment. Int J Biol Macromol. 49(4):747–751.

Sahariah P, Másson M. 2017. Antimicrobial chitosan and chitosan derivatives: a review of the structure-activity Relationship. Biomacromolecules. 18(11):3846–3868. doi:10.1021/acs.biomac.7b01058.

Sahin ZS, Şenöz H, Tezcan H, Büyükgüngör O. 2015. Synthesis, spectral analysis, structural elucidation and

quantum chemical studies of (E)-methyl-4-[(2-phenylhydrazono)methyl]benzoate. Spectrochim Acta A. 143:91–100. doi:10.1016/j.saa.2015.02.032.

Updegraff DM. 1969. Semimicro determination of cellulose in biological materials. Anal Biochem. 32(3):420–424. doi:10.1016/S0003-2697(69)80009-6.

Vanitjinda G, Nimchua T, Sukyai P. 2019. Effect of xylanase-assisted pretreatment on the properties of cellulose and regenerated cellulose films from sugarcane bagasse. Int J Biol Macromol. 122:503–516. doi:10.1016/j.ijbiomac.2018.10.191.

Wang X, Zhang Y, Liang H, Zhou X, Luo Y. 2019. Synthesis and properties of castor oil-based waterborne polyurethane/sodium alginate composites with tunable properties. Carbohydr Polym. 208:391–397. doi:10.1016/j.carbpol.2018.12.090.

Welsh WJ, Tong W, Georgopoulos PG. 2007. Toxicoinformatics: an introduction. In: Ekins S, editor. computational toxicology: risk assessment for pharmaceutical and environmental chemicals. New Jersey: John Wiley & Sons, Inc.; p. 151–181.

Yu S, Xu X, Feng J, Liu M, Hu K. 2019. Chitosan and chitosan coating nanoparticles for the treatment of brain disease. Int J Pharm. 560:282–293. doi:10.1016/j.ijpharm.2019.02.012.